Since January 2020 Elsevier has created a COVID-19 resource centre with free information in English and Mandarin on the novel coronavirus COVID-19. The COVID-19 resource centre is hosted on Elsevier Connect, the company's public news and information website.

European Journal of Medicinal Chemistry 231 (2022) 114130

Contents lists available at ScienceDirect

European Journal of Medicinal Chemistry

journal homepage: http://www.elsevier.com/locate/ejmech

In silico screening-based discovery of novel covalent inhibitors of the SARS-CoV-2 3CL protease

Muya Xiong [a, b, 1], Tianqing Nie [c, 1], Qiang Shao [a], Minjun Li [d], Haixia Su [a, **], Yechun Xu [a, b, c, e, *]

[a] CAS Key Laboratory of Receptor Research and State Key Laboratory of Drug Research, Shanghai Institute of Materia Medica, Chinese Academy of Sciences, Shanghai, 201203, China
[b] University of Chinese Academy of Sciences, Beijing, 100049, China
[c] School of Chinese Materia Medica, Nanjing University of Chinese Medicine, Nanjing, 210023, China
[d] Shanghai Synchrotron Radiation Facility, Shanghai Advanced Research Institute, Chinese Academy of Sciences, Shanghai, 201210, China
[e] School of Pharmaceutical Science and Technology, Hangzhou Institute for Advanced Study, University of Chinese Academy of Sciences, Hangzhou, 310024, China

ARTICLE INFO

Article history:
Received 22 November 2021
Received in revised form
7 January 2022
Accepted 11 January 2022
Available online 23 January 2022

Keywords:
SARS-CoV-2 3C-Like protease
Covalent inhibitor
Virtual screening
Crystal structure

ABSTRACT

The severe acute respiratory syndrome coronavirus 2 (SARS-CoV-2) 3CL protease ($3CL^{pro}$) has been regarded as an extremely promising antiviral target for the treatment of coronavirus disease 2019 (COVID-19). Here, we carried out a virtual screening based on commercial compounds database to find novel covalent non-peptidomimetic inhibitors of this protease. It allowed us to identify 3 hit compounds with potential covalent binding modes, which were evaluated through an enzymatic activity assay of the SARS-CoV-2 $3CL^{pro}$. Moreover, an X-ray crystal structure of the SARS-CoV-2 $3CL^{pro}$ in complex with compound **8**, the most potent hit with an IC_{50} value of 8.50 μM, confirmed the covalent binding of the predicted warhead to the catalytic residue C145, as well as portrayed interactions of the compound with S1' and S2 subsites at the ligand binding pocket. Overall, the present work not merely provided an experiment-validated covalent hit targeting the SARS-CoV-2 $3CL^{pro}$, but also displayed a prime example to seeking new covalent small molecules by a feasible and effective computational approach.

1. Introduction

Since coronavirus disease 2019 (COVID-19) caused by the severe acute respiratory syndrome coronavirus 2 (SARS-CoV-2) became prevalent in the world [1,2], more than 249 million confirmed cases including 5 million deaths have been reported up to 8th November, 2021 (https://covid19.who.int). Although several vaccines targeting the spike protein, two inhibitors of the SARS-CoV-2 RNA-dependent RNA polymerase (RdRp), remdesivir and molnupiravir, together with an inhibitor of the SARS-CoV-2 3C-like protease ($3CL^{pro}$), nirmatrelvir [PF-07321332], have been approved to combat SARS-CoV-2 [3–6], it still needs to find much more therapeutic interventions for this global pandemic. A chymotrypsin-like protease called $3CL^{pro}$, also referred to as the main protease, is a prominent protease which cleaves polyproteins to generate mature nonstructural proteins involved in the replication and transcription of coronaviruses [7,8]. Besides, the rigorous specificity for recognizing the P1-Gln substrate residue at the cleavage site endows the high conservation of the ligand binding site of $3CL^{pro}$ among known coronaviruses [9–11]. Hence, $3CL^{pro}$ has been regarded as a pivotal therapeutic target for treating COVID-19 and other coronavirus-caused diseases [12], and accordingly, the development of $3CL^{pro}$ inhibitors has attracted much attention from medicinal chemists and pharmaceutical industry [13–17].

Currently, the majority of available $3CL^{pro}$ inhibitors are peptidomimetic compounds [18–20], which were designed by the addition of a covalent warhead to a substrate mimic. The known SARS-CoV-2 $3CL^{pro}$ inhibitors like N3 [9,13], 11a [16], 13b [14], PF-00835231 [21], PF-07321332 [6], and the TGEV $3CL^{pro}$ inhibitor such as Cbz-VNSTLQ-CMK [22], contain a warhead of Michael acceptor, aldehyde, α-ketoamide, hydroxymethylketone, nitrile,

* Corresponding author. CAS Key Laboratory of Receptor Research and State Key Laboratory of Drug Research, Shanghai Institute of Materia Medica, Chinese Academy of Sciences, Shanghai 201203, China.
** Corresponding author.
E-mail addresses: suhaixia1@simm.ac.cn (H. Su), ycxu@simm.ac.cn (Y. Xu).
[1] These authors contributed equally to this study.

https://doi.org/10.1016/j.ejmech.2022.114130
0223-5234/

and chloromethyl ketone, respectively. In contrast, non-peptidomimetic inhibitors have been rather derived from high-throughput screening/virtual screening of repurposing drugs/natural products/compound database [23—25]. Given that the presence of the covalent warhead endows the superiority in prolonged residence time [26] and it is a big challenge to improve the oral bioavailability of peptidomimetic inhibitors, non-peptidomimetic small-molecule inhibitors carrying covalent warheads may offer an opportunity to facilitate the discovery of more potent and drug-like 3CL^{pro} inhibitors.

Several SARS-CoV-2 3CL^{pro} non-peptidomimetic covalent inhibitors like ebselen [13], PX-12 [13], carmofur [23], myricetin [25], and ester derivatives [27] have been identified mostly by the high-throughput screening. However, there are very few studies that such inhibitors were uncovered or designed with the aid of computational approaches. Recently, Zaidman, et al. [28] successfully employed a computational pipeline, *covalentizer*, to design a low micromolar covalent SARS-CoV-2 3CL^{pro} inhibitor by adding an acrylamide warhead to a non-covalent inhibitor, ML188. Similarly, Stille, et al. [29] utilized the docking program FITTED to convert a non-covalent inhibitor of the SARS-CoV 3CL^{pro} (X77) to a sub-micromolar covalent inhibitor by replacing the imidazole group with a covalent warhead. In addition, a covalent virtual screening on an in-house database of small pseudopeptides with Michael acceptors yielded two SARS-CoV-2 3CL^{pro} inhibitors, albeit with the relatively low potency [30].

In this work, we collected covalent warheads observed among the known peptidomimetic inhibitors of the SARS-CoV-2 3CL^{pro} and used them as reference to pick up the potential covalent binders from the list resulting from the virtual screening on ChemDiv database. A covalent molecular docking was further performed on these selected potential covalent binders. Finally, we purchased eight compounds for testing their enzymatic activities against the SARS-CoV-2 3CL^{pro}, and yielded three novel-scaffold hits with different warheads. The X-ray crystal structure of the SARS-CoV-2 3CL^{pro} in complex with the most effective compound (**8**) revealed the covalent binding mode, and the intrinsic reactivity of its warhead was explored through a glutathione (GSH) assay, providing a basis for further optimization. Accordingly, our study demonstrated that the strategy of a virtual screening followed by a covalent molecular docking is able to quickly identify the novel covalent inhibitors of the SARS-CoV-2 3CL^{pro}.

2. Materials and Methods

2.1. Virtual screening

Our protocol for in silico screening consisted of two stages: a large-scale non-covalent virtual screening of compounds from ChemDiv database, which was followed by a covalent docking of the compounds containing the warheads shown in Fig. 1. We used tools implemented in the Schrödinger 2015 suite to carry out the virtual screening with the crystal structure of SARS-CoV-2 3CL^{pro} in complex with myricetin (PDB ID: 7B3E) as the receptor structure. The receptor was prepared using the Protein Preparation Wizard [31] to add hydrogen atoms and the missing residue side chains. The covalent bond formed between the catalytic C145 and myricetin was broken for proceeding with non-covalent virtual screening in the first stage. The overall structure was refined using OPLS3 forced field [32] with harmonic restraints on heavy atoms.

The receptor grid was centered on the centroid of myricetin and generated using the Receptor Grid Generation to define the binding site for ligand docking. Subsequently, a virtual screening was performed using Virtual Screening Workflow (Fig. 1). The three-dimensional (3D) structures of ~1,500,000 compounds from the

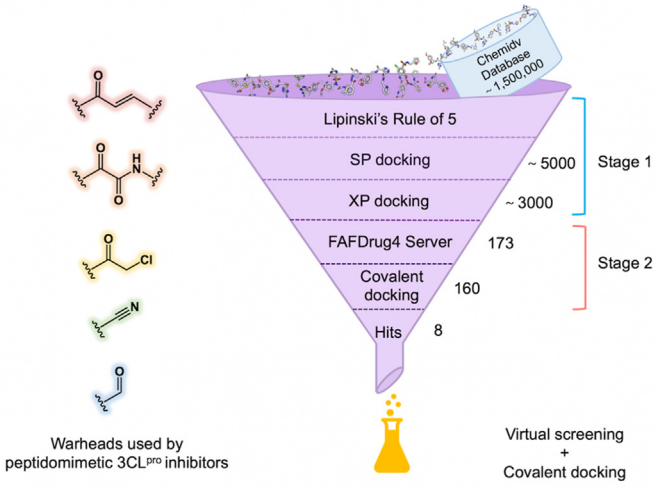

Fig. 1. Workflow of a virtual screening followed by a covalent molecular docking for discovery of covalent SARS-CoV-2 3CL^{pro} inhibitors.

database were yielded with LigPrep. The overall workflow included filtering the prepared structures of compounds with Propfilter and docking them to the receptor grid using Glide. In the filtering step, we filtered out compounds that are not compatible with Lipinski's Rule of 5. In the docking step, we carried out standard precision (SP) docking with default settings. The top 5000 docked compounds were then reserved for the extra precision (XP) docking and the 3000 highest-ranking compounds out of them were retained for covalent docking in the second stage.

2.2. Covalent docking

Using FAF-Drug4 Server [33], 173 compounds containing potential covalent warheads were first selected from 3000 compounds which were collected from the non-covalent virtual screening. Furthermore, 160 compounds containing five different types of warheads including chloromethyl ketone, Michael acceptor, aldehyde, nitrile, and alpha-ketoamide, which are widely applied in the reported 3CL^{pro} inhibitors [10,18,20] and also easy to be synthesized, were selected, and their 3D structures were produced using LigPrep.

The structure of SARS-CoV-2 3CL^{pro}-myricetin complex as mentioned above was used as the receptor structure, and the protease-inhibitor covalent bond was maintained for the following covalent docking using Covalent Docking [34]. The catalytic C145 was defined as a reactive residue and the centroid of myricetin was used as the box center. The reaction type was determined by the reactive group of the compound. And the covalent docking was performed with a pose prediction mode. The top-ranking compounds were visually checked to find the correct reactive sites as well as binding modes, particularly, to meet the requirement for interacting with the residues in the crucial S1 (F140/N142/G143/H163/E166) or S2 (H41/M49/Q189) subsites as suggested by the structure-activity relationship summarized in our previous review [20]. In the end, we purchased 8 compounds with five types of covalent warheads and different scaffolds from TargetMol for an inhibitory activity test. PF-07321332, a positive control to our enzymatic inhibition assay, was purchased from MedChemExpress.

2.3. Protein expression and purification

The cDNA of SARS-CoV-2 3CL^{pro} (Gen-Bank: MN908947.3) with a N-terminal SUMO tag was cloned into the pET-15b vector. The

plasmid was then transformed into BL21 (DE3) cells for protein expression. The expressed protein was purified by a Ni-NTA column (GE Healthcare) and cleaved by the SUMO specific peptidase 2 (SENP2) to remove the SUMO tag. The resulting protein sample was further purified by Q-Sepharose followed by a size-exclusion chromatography (GE Healthcare). The eluted protein samples were stored in a solution (10 mM Tris, pH 7.5) for the enzymatic inhibition assay and protein crystallization.

2.4. Enzymatic inhibition assay of SARS-CoV-2 3CL^{pro}

A fluorescence resonance energy transfer (FRET) protease assay was applied to measure the inhibitory activity of compounds against the SARS-CoV-2 3CL^{pro} [24,25]. The fluorogenic substrate (MCA-AVLQSGFR-Lys(Dnp)-Lys-NH2) was synthesized by GenScript (Nanjing, China). The FRET-based protease assay was performed as follows. The recombinant SARS-CoV-2 3CL^{pro} (50 nM at a final concentration) was mixed with serial dilutions of each compound in 80 μL assay buffer (50 mM Tris, pH 7.3, 1 mM EDTA) and incubated for 30 min. The reaction was initiated by adding 40 μL fluorogenic substrate with a final concentration of 20 μM. After that, the fluorescence signal at 320 nm (excitation)/405 nm (emission) was immediately measured every 30 s for 5 min with a Bio-Tek Synergy-H1 plate reader. The initial velocity of reactions added with compounds compared to the reaction added with DMSO were calculated and used to generate IC_{50} curves.

2.5. Protein crystallization and structure determination

The purified SARS-CoV-2 3CL^{pro} protein was concentrated to 9 mg/mL for crystallization. To obtain complex structures, the SARS-CoV-2 3CL^{pro} protein was incubated with 8 mM compound **8** for 1 h before crystallization condition screening. Crystals of the complex was obtained under the condition of 10−25% PEG6000, 100 mM MES, pH 5.75−6.25, and 3% DMSO. Crystals were flash frozen in liquid nitrogen in the presence of the reservoir solution supplemented with 20% glycerol. X-ray diffraction data were collected at beamline BL18U1 at the Shanghai Synchrotron Radiation Facility [35]. Bluice was used to collect X-ray diffraction data. The data were processed with HKL3000 software packages [36]. The complex structures were solved by molecular replacement using the program PHASER [37] with a search model of PDB code 6M2N [24]. The model was built using Coot [38] and refined with the program PHENIX [39]. The refined structure was deposited to Protein Data Bank with the accession code listed in Table 1. The complete statistics as well as the quality of the solved structure are also shown in Table 1.

2.6. Half-life determination of hits reacting with GSH

The reaction rates of the compounds with GSH were measured with the previous reported protocol [40]. The compounds **2**, **3** and **8** at a final concentration of 400 μM were incubated with 10 μM GSH in potassium phosphate buffer, respectively. 7-diethylamino-3-(4'-maleimidylphenyl)-4-methylcoumarin (CPM, ThermoFisher) at a concentration of 50 μM was added to the reaction system at definite time (2.5, 5, 10, 20, 40, 60, and 80 min) to quantify the remaining GSH. After that, the fluorescence signal at 384 nm (excitation)/470 nm (emission) was immediately measured using a Bio-Tek Synergy-H1 plate reader. Ln (the percentage of the remaining compounds) was plotted against incubation time to generate the half-life time of the compound reacting with GSH.

Table 1
Crystallography data collection and refinement statistics.

	SARS-CoV-2 3CL^{pro}-**8**
PDB ID	7VVT
Space Group	$P\,2_12_12_1$
Cell Dimension: a (Å)	67.99
b (Å)	90.12
c (Å)	103.17
Wavelength (Å)	0.9785
Reflections (unique)	22010
Resolution Range (Å)	26.25−2.51
Highest-Resolution Shell (Å)	2.62−2.51
Redundancy	12.7
I/σ (I)	0.75 (2.51 Å)
Completeness (%)	99.2 (99.5)
Rwork/Rfree	0.2339/0.2527
Clashscore	0.96
MolProbity Score	0.79
RMS Values	
Bond length (Å)	0.003
Bond angle (°)	0.631
Numbers of Non-hydrogen Atoms	
Protein	4234
Inhibitor	42
Water Oxygen	55
Others	0
Ramachandran plot	
Favored (%)	98.61
Allowed (%)	1.22
Outliers (%)	0.17

3. Results and discussion

3.1. Evaluation of virtual screened hits by the enzymatic inhibition assay

As described in Materials and Methods, 8 compounds resulting from the non-covalent virtual screening and covalent docking were subject to the experimental validation using a FRET protease assay. In the initial test at a concentration of 50 μM, 3 of 8 compounds (**2**, **3** and **8**) displayed over 50% inhibition towards the SARS-CoV-2 3CL^{pro} (Fig. 2A and Table 2). A nitrile, Michael acceptor and chloromethyl ketone are the warheads included in compounds **2**, **3** and **8**, respectively. The determined IC_{50} values of these three compounds are 19.09, 36.07 and 8.50 μM, respectively (Fig. 2B−D) and the IC_{50} value of PF-07321332 (0.054 μM), a covalent peptidomimetic inhibitor of the SARS-CoV-2 3CL^{pro} recently approved by the FDA [6], is also determined (Table 2).

3.2. A crystal structure of the SARS-CoV-2 3CL^{pro} in complex with compound ***8***

We then sought to determine crystal structures of the SARS-CoV-2 3CL^{pro} in complex with 3 hit compounds in order to elucidate the precise protease-ligand binding mode. What's more, it also would be revealed directly whether these hits are covalent inhibitors or not. As a result, the crystal structure of the SARS-CoV-2 3CL^{pro} bound with compound **8**, the best inhibitor among three compounds (IC_{50} = 8.50 μM), was determined. As expected, the methylene group of the chloromethyl ketone moiety was attacked by the catalytic C145 to form a C−S covalent bond, supported by continuous electron density map between the inhibitor and the residue (Fig. 3A). Besides, the carbonyl group of the chloromethyl ketone established a hydrogen-bond (H-bond) with the main chain of G143, and a π−π stacking interaction occurred between the benzene ring and the side chain of the other catalytic residue H41. Especially, a *meta* chloro-substitution (*m*-Cl) of the benzene ring formed a rare halogen-bond with the sulfur atom of M165 (Fig. 3B).

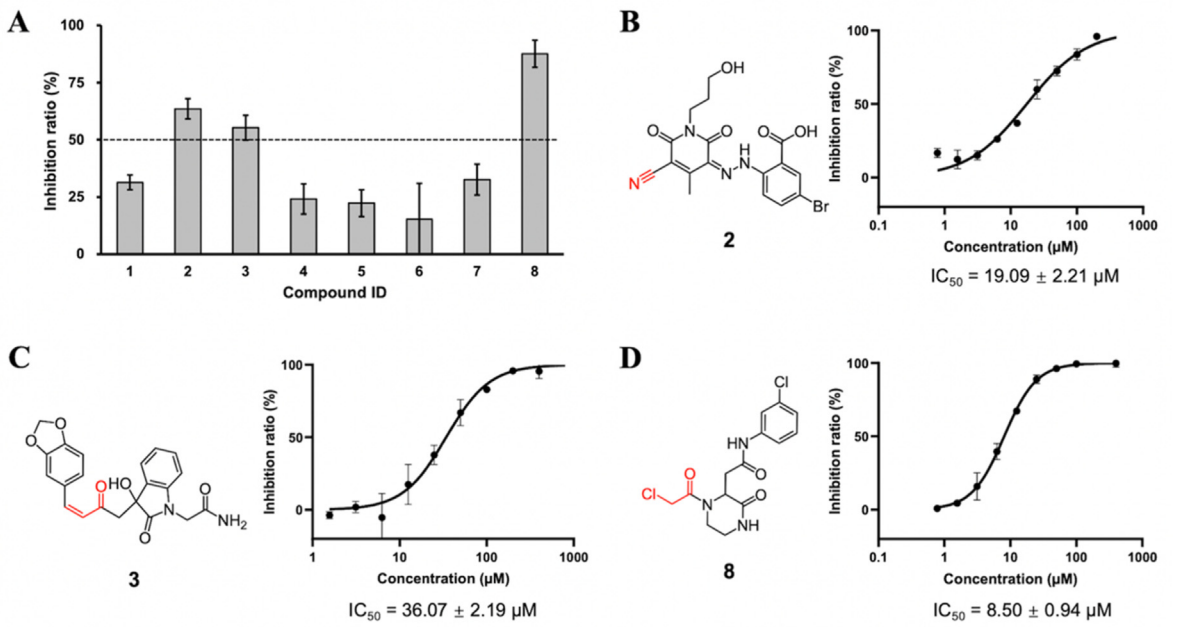

Fig. 2. Inhibition of the enzymatic activity of the SARS-CoV-2 $3CL^{pro}$ by hit compounds. (A) Inhibition of 8 compounds against the SARS-CoV-2 $3CL^{pro}$. Chemical structures, concentration-dependent inhibitory profiles against the protease and the resulting IC_{50} values of (B) **2**, (C) **3**, and (D) **8**. Error bars represent mean ± SD of three independent experiments.

Thus, the inhibitory activity of compound **8** against the SARS-CoV-2 $3CL^{pro}$ was an integrated result of the covalent bonding and non-covalent binding interactions.

The substrate binding site of the SARS-CoV-2 $3CL^{pro}$ is normally divided into S1′, S1, S2, and S4 subsites [10,15]. As shown in Fig. 3C, compound **8** mainly occupied the S1' and S2 subsites. Particularly, the highly plastic S2 subsite, featured with the flexible Q189 in the SARS-CoV $3CL^{pro}$ [41], perfectly accommodated the *m*-Cl substituted benzene ring of **8**, making it to be sandwiched between H41 and Q189 (Fig. 3D). It is well acknowledged that the S1 subsite of $3CL^{pro}$ specifically recognizes the P1-Gln of the substrate so that almost all the peptidomimetic $3CL^{pro}$ inhibitors used mimics of glutamine to interact with the S1 subsite [42,43]. Such a strategy could also be utilized in the optimization of compound **8** to pursuit the higher potency.

3.3. The binding modes of compounds *2* and *3* with the protease predicted by covalent docking

Since all attempts failed to determine crystal structures of the protease bound with compound **2** or **3**, their possible covalent binding modes were carefully studied by the covalent docking. Owning to the anchoring of the nitrile warhead of compound **2** to C145 in the active site, the carbonyl group of 2,6-dioxo-1,2,3,6-tetrahydropyridine close to the warhead pointed to the oxyanion hole so as to stabilize a reaction intermediate, making H-bonding with the backbone nitrogen atoms of G143, S144 and C145 (Fig. 4A). Additionally, other substituents of the tetrahydropyridine were bridged by H-bonds with the backbone of E166 as well as the side chain of N142. For compound **3**, a Michael acceptor warhead covalently interacted with C145. In addition, it also established H-bonds with the main chain of G143 and E166, the side chain of N142, and the side chain of Q189 (Fig. 4B).

Accordingly, both compounds **2** and **3** mainly occupied the S1′ and S1 subsites (Fig. 4C and D), which is distinct to the binding pose of compound **8** described above. Moreover, the 5-bromo-benzoic acid group of compound **2** reached into the S2 and S4 subsites, while the benzo[d] [1,3]dioxole group of compound **3** was only located at the border of S1', S2 and S4 without protruding into any of these subsites (Fig. 4C and D).

3.4. The reactivity of 3 hits with the SARS-CoV-2 $3CL^{pro}$

Generally speaking, the reactivity of covalent inhibitors with the targeted cysteine is crucial for covalent drug development, considering that the hyper-reactivity of the warheads may trigger potential side effects, e.g., drug-induced toxicity or immunogenicity [44,45]. Consequently, the reactivity of three hit compounds was measured by a GSH assay which is usually used to estimate the reactivity of cysteine-targeted warheads [46]. The resulting half-lives ($t_{1/2}$) of compounds **3** and **8** were 103 and 90 min, respectively, while that of compound **2** was less than 2.5 min (Fig. 5). Referring to the fact that $t_{1/2}$s of covalent kinase inhibitors in clinics are often in the range of 30–512 min [47], compounds **3** and **8** demonstrated the moderate reactivity, providing the feasibility for further development of more potent covalent inhibitors of the protease. The nitrile warhead of compound **2**, on the other hand, showed much higher reactivity, presumably because of the nearby several electron withdrawing groups.

4. Conclusions

In the present work, the strategy of a non-covalent virtual screening combined with a covalent docking was utilized to seek out novel covalent non-peptidomimetic inhibitors of the SARS-CoV-2 $3CL^{pro}$. Based on the results from such a combined screening, we purchased eight compounds with five types of covalent warheads which were previously reported in covalent peptidomimetic inhibitors of $3CL^{pro}$. Following the validation of the enzyme inhibition, we succeeded in unveiling three hits with IC_{50} values of 19.09, 36.07 and 8.50 μM, respectively. Coincidentally, these active compounds, namely compounds **2**, **3** and **8**, were

Table 2
The inhibition activity of 8 compounds and PF-07321332 against the SARS-CoV-2 $3CL^{pro}$.

Compd.		Structure	M.W.	Inhibitory Ratio (%) (@50 μM)	IC_{50} (μM) ± SD[a]
ID	ChemDiv ID				
1	L793-0077	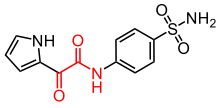	293.30	31.37 ± 0.70	–
2	5646–1357	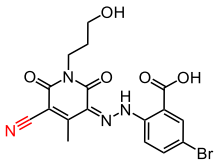	435.23	65.53 ± 1.39	19.09 ± 2.21
3	6225–0388	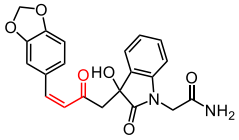	394.38	55.24 ± 0.56	36.07 ± 2.19
4	8015–3451	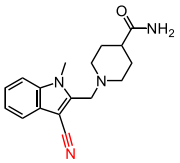	296.37	24.11 ± 6.50	–
5	D009-0584	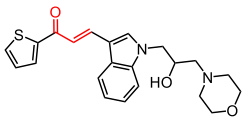	396.50	22.26 ± 3.78	–
6	D360-7047	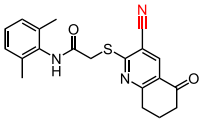	365.45	15.25 ± 14.78	–
7	K788-4271	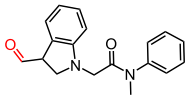	292.34	32.60 ± 5.22	–
8	Y020-9948	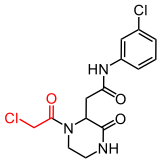	344.20	87.56 ± 4.66	8.50 ± 0.94
PF-07321332		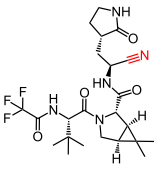	499.53	–	0.054 ± 0.002

[a] Each value is the mean ± SD of three independent experiments.

armed with three divergent covalent warheads including nitrile, Michael acceptor, and chloromethyl ketone. Remarkably, the crystal structure determination of the $3CL^{pro}$-**8** complex depicted that compound **8** covalently binds to C145 and meanwhile non-covalently interacts with residues of the S1′ and S2 subsites. In contrast, compounds **2** and **3** were predicted to mainly interact with the S1' and S1 subsites. Furthermore, the reactivity of 3 hits evaluated by the GSH assay demonstrated that the warheads of

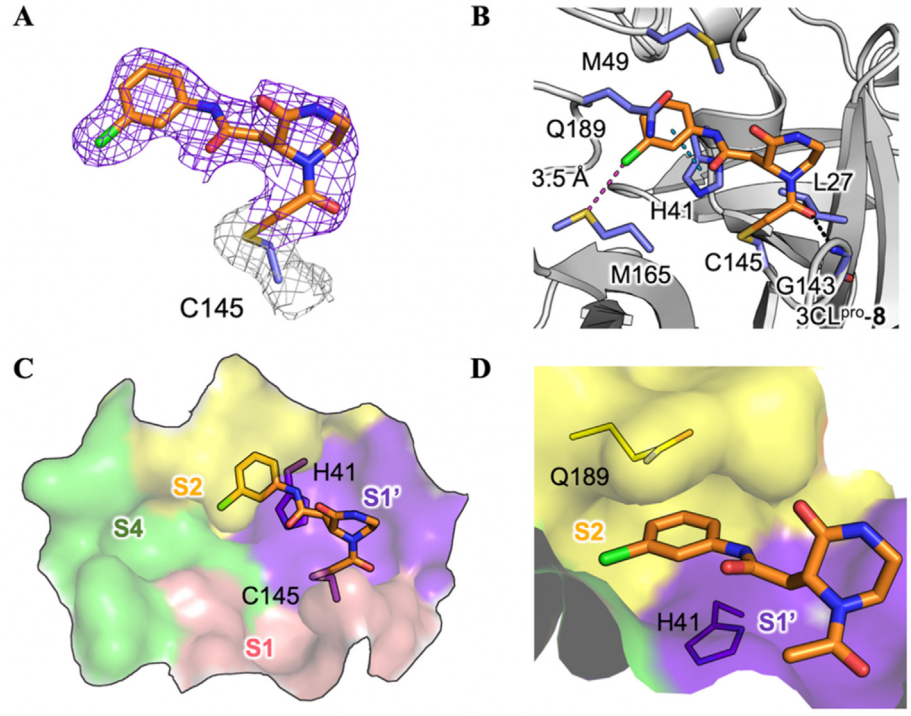

Fig. 3. Crystal structure of the SARS-CoV-2 $3CL^{pro}$ in complex with compound **8**. (A) A $2F_o$-F_c density map of compound **8** and residue C145 contoured at 1.0 σ are shown in purple and light grey meshes. (B) The binding mode of **8** with the SARS-CoV-2 $3CL^{pro}$. The protease is rendered in grey cartoon, compound **8** is shown in orange sticks, and the surrounding residues are displayed with light-purple sticks. H-bonding, π-π stacking and halogen-bonding interactions are represented by black, blue and purple dashed lines, respectively. A molecular surface representation of compound **8** interacting with the S1′-S4 subsites of the protease in a (C) top view and (D) front view. The subsites are colored purple (S1′), pink (S1), yellow (S2), and green (S4). The catalytic dyad of the protease (C145 and H41) is shown in sticks.

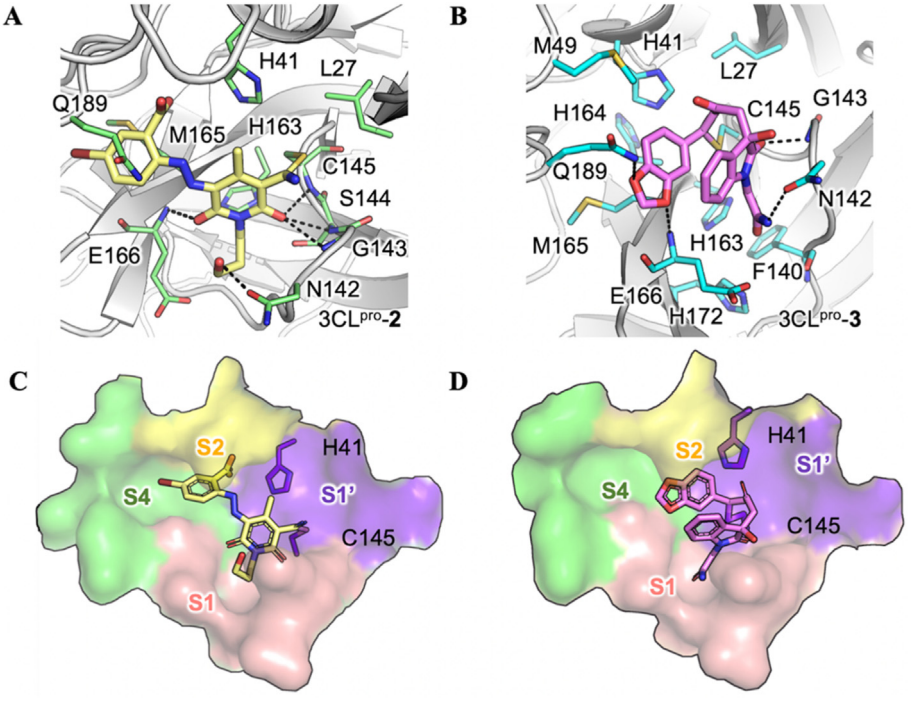

Fig. 4. Docked binding modes of compounds **2** and **3** with the SARS-CoV-2 $3CL^{pro}$. The binding modes of compounds (A) **2** and (B) **3** with the SARS-CoV-2 $3CL^{pro}$ predicted by the covalent docking. The protease is shown in white cartoon, compounds are shown in yellow and violet sticks, and the surrounding residues are shown in green and cyan sticks. H-bonds are represented by black dashed lines. A molecular surface representation of (C) **2** and (D) **3** interacting with S1′-S4 subsites of $3CL^{pro}$ from a top view. The subsites are colored purple (S1′), pink (S1), yellow (S2), and green (S4). The catalytic dyad is shown in sticks.

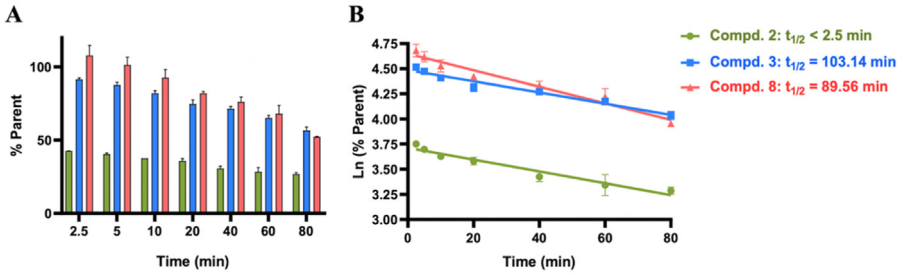

Fig. 5. Half-life determination of 3 hits reacting with GSH. (A) Compounds **2**, **3** and **8** (at a final concentration of 400 μM) was incubated with 10 μM GSH for 2.5, 5, 10, 20, 40, 60, and 80 min, in the presence of oxygen. (B) Ln (the percentage of the remaining compounds) was plotted against incubation time to characterize the half-life time of compounds reacting with GSH.

compounds **3** and **8** have the moderate reactivity to GSH, rendering them to be further developed as potent covalent inhibitors of the protease. Overall, the identified compound **8** provided a good starting point for the discovery of novel covalent non-peptidomimetic inhibitors of the SARS-CoV-2 $3CL^{pro}$, and the covalent docking offers an efficient and feasible strategy for discovery of novel covalent binders.

Declaration of competing interest

The authors declare that they have no known competing financial interests or personal relationships that could have appeared to influence the work reported in this paper.

Acknowledgments

We thank the staff from BL18U1 beamline of National Facility for Protein Science in Shanghai (NFPS) at Shanghai Synchrotron Radiation Facility, for assistance during data collection. This work was supported by the National Natural Science Foundation of China (No. 21877122 and No. 32071248), the Science and Technology Commission of Shanghai Municipality (No. 20430780300 and No. 19431901100), and the Sustainable Development of Precious Traditional Chinese Medicine Resources (No. 2060302-2001-01).

References

[1] L. Perico, A. Benigni, F. Casiraghi, L.F.P. Ng, L. Renia, G. Remuzzi, Immunity, endothelial injury and complement-induced coagulopathy in COVID-19, Nat. Rev. Nephrol. 17 (2021) 46–64.
[2] C. Wang, P.W. Horby, F.G. Hayden, G.F. Gao, A novel coronavirus outbreak of global health concern, Lancet 395 (2020) 470–473.
[3] M. Wang, R. Cao, L. Zhang, X. Yang, J. Liu, M. Xu, Z. Shi, Z. Hu, W. Zhong, G. Xiao, Remdesivir and chloroquine effectively inhibit the recently emerged novel coronavirus (2019-nCoV) in vitro, Cell Res. 30 (2020) 269–271.
[4] J.H. Beigel, K.M. Tomashek, L.E. Dodd, A.K. Mehta, B.S. Zingman, A.C. Kalil, E. Hohmann, H.Y. Chu, A. Luetkemeyer, S. Kline, D.L. de Castilla, R.W. Finberg, K. Dierberg, V. Tapson, L. Hsieh, T.F. Patterson, R. Paredes, D.A. Sweeney, W.R. Short, G. Touloumi, D.C. Lye, N. Ohmagari, M.D. Oh, G.M. Ruiz-Palacios, T. Benfield, G. Fatkenheuer, M.G. Kortepeter, R.L. Atmar, C.B. Creech, J. Lundgren, A.G. Babiker, S. Pett, J.D. Neaton, T.H. Burgess, T. Bonnett, M. Green, M. Makowski, A. Osinusi, S. Nayak, H.C. Lane, A.-S. Grp, Remdesivir for the treatment of COVID-19-final report, N. Engl. J. Med. 383 (2020) 1813–1826.
[5] A. Jayk Bernal, M.M. Gomes da Silva, D.B. Musungaie, E. Kovalchuk, A. Gonzalez, V. Delos Reyes, A. Martin-Quiros, Y. Caraco, A. Williams-Diaz, M.L. Brown, J. Du, A. Pedley, C. Assaid, J. Strizki, J.A. Grobler, H.H. Shamsuddin, R. Tipping, H. Wan, A. Paschke, J.R. Butterton, M.G. Johnson, C. De Anda, M.O.-O.S. Group, Molnupiravir for oral treatment of covid-19 in nonhospitalized patients, N. Engl. J. Med. (2021), https://doi.org/10.1056/NEJMoa2116044.
[6] D.R. Owen, C.M.N. Allerton, A.S. Anderson, L. Aschenbrenner, M. Avery, S. Berritt, B. Boras, R.D. Cardin, A. Carlo, K. Coffman, A. Dantonio, L. Di, H. Eng, R. Ferre, K.S. Gajiwala, S.A. Gibson, S.E. Greasley, B.L. Hurst, E.P. Kadar, A.S. Kalgutkar, J.C. Lee, J. Lee, W. Liu, S.W. Mason, S. Noell, J.J. Novak, R.S. Obach, K. Ogilvie, N.C. Patel, M. Pettersson, D.K. Rai, M.R. Reese, M.F. Sammons, J.G. Sathish, R.S.P. Singh, C.M. Steppan, A.E. Stewart, J.B. Tuttle, L. Updyke, P.R. Verhoest, L. Wei, Q. Yang, Y. Zhu, An oral SARS-CoV-2 M^{pro} inhibitor clinical candidate for the treatment of COVID-19, Science 374 (2021) 1586–1593.
[7] M.D. Sacco, C. Ma, P. Lagarias, A. Gao, J.A. Townsend, X. Meng, P. Dube, X. Zhang, Y. Hu, N. Kitamura, B. Hurst, B. Tarbet, M.T. Marty, A. Kolocouris, Y. Xiang, Y. Chen, J. Wang, Structure and inhibition of the SARS-CoV-2 main protease reveal strategy for developing dual inhibitors against M^{pro} and cathepsin L, Sci. Adv. 6 (2020), eabe0751.
[8] R.L. Hoffman, R.S. Kania, M.A. Brothers, J.F. Davies, R.A. Ferre, K.S. Gajiwala, M. He, R.J. Hogan, K. Kozminski, L.Y. Li, J.W. Lockner, J. Lou, M.T. Marra, L.J. Mitchell Jr., B.W. Murray, J.A. Nieman, S. Noell, S.P. Planken, T. Rowe, K. Ryan, G.J. Smith 3rd, J.E. Solowiej, C.M. Steppan, B. Taggart, Discovery of ketone-based covalent inhibitors of coronavirus 3CL proteases for the potential therapeutic treatment of COVID-19, J. Med. Chem. 63 (2020) 12725–12747.
[9] H. Yang, W. Xie, X. Xue, K. Yang, J. Ma, W. Liang, Q. Zhao, Z. Zhou, D. Pei, J. Ziebuhr, R. Hilgenfeld, K.Y. Yuen, L. Wong, G. Gao, S. Chen, Z. Chen, D. Ma, M. Bartlam, Z. Rao, Design of wide-spectrum inhibitors targeting coronavirus main proteases, PLoS Biol. 3 (2005), e324.
[10] T. Pillaiyar, M. Manickam, V. Namasivayam, Y. Hayashi, S.H. Jung, An overview of Severe Acute Respiratory Syndrome-Coronavirus (SARS-CoV) 3CL protease inhibitors: peptidomimetics and small molecule chemotherapy, J. Med. Chem. 59 (2016) 6595–6628.
[11] Z. Ren, L. Yan, N. Zhang, Y. Guo, C. Yang, Z. Lou, Z. Rao, The newly emerged SARS-like coronavirus HCoV-EMC also has an "Achilles' heel": current effective inhibitor targeting a 3C-like protease, Protein Cell 4 (2013) 248–250.
[12] C. Liu, Q. Zhou, Y. Li, L.V. Garner, S.P. Watkins, L.J. Carter, J. Smoot, A.C. Gregg, A.D. Daniels, S. Jervey, D. Albaiu, Research and development on therapeutic agents and vaccines for COVID-19 and related human coronavirus diseases, ACS Cent. Sci. 6 (2020) 315–331.
[13] Z.M. Jin, X.Y. Du, Y.C. Xu, Y.Q. Deng, M.Q. Liu, Y. Zhao, B. Zhang, X.F. Li, L.K. Zhang, C. Peng, Y.K. Duan, J. Yu, L. Wang, K.L. Yang, F.J. Liu, R.D. Jiang, X.L. Yang, T. You, X.C. Liu, X.N. Yang, F. Bai, H. Liu, X. Liu, L.W. Guddat, W.Q. Xu, G.F. Xiao, C.F. Qin, Z.L. Shi, H.L. Jiang, Z.H. Rao, H.T. Yang, Structure of M^{pro} from SARS-CoV-2 and discovery of its inhibitors, Nature 582 (2020) 289–293.
[14] L. Zhang, D. Lin, X. Sun, U. Curth, C. Drosten, L. Sauerhering, S. Becker, K. Rox, R. Hilgenfeld, Crystal structure of SARS-CoV-2 main protease provides a basis for design of improved alpha-ketoamide inhibitors, Science 368 (2020) 409–412.
[15] J.X. Qiao, Y.S. Li, R. Zeng, F.L. Liu, R.H. Luo, C. Huang, Y.F. Wang, J. Zhang, B.X. Quan, C.J. Shen, X. Mao, X.L. Liu, W.N. Sun, W. Yang, X.C. Ni, K. Wang, L. Xu, Z.L. Duan, Q.C. Zou, H.L. Zhang, W. Qu, Y.H.P. Long, M.H. Li, R.C. Yang, X.L. Liu, J. You, Y.L. Zhou, R. Yao, W.P. Li, J.M. Liu, P. Chen, Y. Liu, G.F. Lin, X. Yang, J. Zou, L.L. Li, Y.G. Hu, G.W. Lu, W.M. Li, Y.Q. Wei, Y.T. Zheng, J. Lei, S.Y. Yang, SARS-CoV-2 M^{pro} inhibitors with antiviral activity in a transgenic mouse model, Science 371 (2021) 1374–1378.
[16] W. Dai, B. Zhang, X.M. Jiang, H. Su, J. Li, Y. Zhao, X. Xie, Z. Jin, J. Peng, F. Liu, C. Li, Y. Li, F. Bai, H. Wang, X. Cheng, X. Cen, S. Hu, X. Yang, J. Wang, X. Liu, G. Xiao, H. Jiang, Z. Rao, L.K. Zhang, Y. Xu, H. Yang, H. Liu, Structure-based design of antiviral drug candidates targeting the SARS-CoV-2 main protease, Science 368 (2020) 1331–1335.
[17] S. Gunther, P.Y.A. Reinke, Y. Fernandez-Garcia, J. Lieske, T.J. Lane, H.M. Ginn, F.H.M. Koua, C. Ehrt, W. Ewert, D. Oberthuer, O. Yefanov, S. Meier, K. Lorenzen, B. Krichel, J.D. Kopicki, L. Gelisio, W. Brehm, I. Dunkel, B. Seychell, H. Gieseler, B. Norton-Baker, B. Escudero-Perez, M. Domaracky, S. Saouane, A. Tolstikova, T.A. White, A. Hanle, M. Groessler, H. Fleckenstein, F. Trost, M. Galchenkova, Y. Gevorkov, C. Li, S. Awel, A. Peck, M. Barthelmess, F. Schlunzen, P. Lourdu Xavier, N. Werner, H. Andaleeb, N. Ullah, S. Falke, V. Srinivasan, B.A. Franca, M. Schwinzer, H. Brognaro, C. Rogers, D. Melo, J.J. Zaitseva-Doyle, J. Knoska, G.E. Pena-Murillo, A.R. Mashhour, V. Hennicke, P. Fischer, J. Hakanpaa, J. Meyer, P. Gribbon, B. Ellinger, M. Kuzikov, M. Wolf, A.R. Beccari, G. Bourenkov, D. von Stetten, G. Pompidor, I. Bento, S. Panneerselvam, I. Karpics, T.R. Schneider, M.M. Garcia-Alai, S. Niebling, C. Gunther, C. Schmidt, R. Schubert, H. Han, J. Boger, D.C.F. Monteiro, L. Zhang, X. Sun, J. Pletzer-

Zelgert, J. Wollenhaupt, C.G. Feiler, M.S. Weiss, E.C. Schulz, P. Mehrabi, K. Karnicar, A. Usenik, J. Loboda, H. Tidow, A. Chari, R. Hilgenfeld, C. Uetrecht, R. Cox, A. Zaliani, T. Beck, M. Rarey, S. Gunther, D. Turk, W. Hinrichs, H.N. Chapman, A.R. Pearson, C. Betzel, A. Meents, X-ray screening identifies active site and allosteric inhibitors of SARS-CoV-2 main protease, Science 372 (2021) 642–646.

[18] T. Pillaiyar, S. Meenakshisundaram, M. Manickam, Recent discovery and development of inhibitors targeting coronaviruses, Drug Discov. Today 25 (2020) 668–688.

[19] Y. Liu, C. Liang, L. Xin, X. Ren, L. Tian, X. Ju, H. Li, Y. Wang, Q. Zhao, H. Liu, W. Cao, X. Xie, D. Zhang, Y. Wang, Y. Jian, The development of Coronavirus 3C-Like protease (3CL(pro)) inhibitors from 2010 to 2020, Eur. J. Med. Chem. 206 (2020) 112711.

[20] M.Y. Xiong, H.X. Su, W.F. Zhao, H. Xie, Q. Shao, Y.C. Xu, What coronavirus 3C-like protease tells us: from structure, substrate selectivity, to inhibitor design, Med. Res. Rev. 41 (2021) 1965–1998.

[21] B. Boras, R.M. Jones, B.J. Anson, D. Arenson, L. Aschenbrenner, M.A. Bakowski, N. Beutler, J. Binder, E. Chen, H. Eng, H. Hammond, J. Hammond, R.E. Haupt, R. Hoffman, E.P. Kadar, R. Kania, E. Kimoto, M.G. Kirkpatrick, L. Lanyon, E.K. Lendy, J.R. Lillis, J. Logue, S.A. Luthra, C. Ma, S.W. Mason, M.E. McGrath, S. Noell, R.S. Obach, M.N. O'Brien, R. O'Connor, K. Ogilvie, D. Owen, M. Pettersson, M.R. Reese, T.F. Rogers, M.I. Rossulek, J.G. Sathish, N. Shirai, C. Steppan, M. Ticehurst, L.W. Updyke, S. Weston, Y. Zhu, J. Wang, A.K. Chatterjee, A.D. Mesecar, M.B. Frieman, A.S. Anderson, C. Allerton, Discovery of a novel inhibitor of coronavirus 3CL protease for the potential treatment of COVID-19, bioRxiv (2021), https://doi.org/10.1101/2020.09.12.293498.

[22] K. Anand, J. Ziebuhr, P. Wadhwani, J.R. Mesters, R. Hilgenfeld, Coronavirus main proteinase (3CLpro) structure: basis for design of anti-SARS drugs, Science 300 (2003) 1763–1767.

[23] Z. Jin, Y. Zhao, Y. Sun, B. Zhang, H. Wang, Y. Wu, Y. Zhu, C. Zhu, T. Hu, X. Du, Y. Duan, J. Yu, X. Yang, X. Yang, K. Yang, X. Liu, L.W. Guddat, G. Xiao, L. Zhang, H. Yang, Z. Rao, Structural basis for the inhibition of SARS-CoV-2 main protease by antineoplastic drug carmofur, Nat. Struct. Mol. Biol. 27 (2020) 529–532.

[24] H.X. Su, S. Yao, W.F. Zhao, M.J. Li, J. Liu, W.J. Shang, H. Xie, C.Q. Ke, H.C. Hu, M.N. Gao, K.Q. Yu, H. Liu, J.S. Shen, W. Tang, L.K. Zhang, G.F. Xiao, L. Ni, D.W. Wang, J.P. Zuo, H.L. Jiang, F. Bai, Y. Wu, Y. Ye, Y.C. Xu, Anti-SARS-CoV-2 activities in vitro of Shuanghuanglian preparations and bioactive ingredients, Acta Pharmacol. Sin. 41 (2020) 1167–1177.

[25] H.X. Su, S. Yao, W.F. Zhao, Y.M. Zhang, J. Liu, Q. Shao, Q.X. Wang, M.J. Li, H. Xie, W.J. Shang, C.Q. Ke, L. Feng, X.R. Jiang, J.S. Shen, G.F. Xiao, H.L. Jiang, L.K. Zhang, Y. Ye, Y.C. Xu, Identification of pyrogallol as a warhead in design of covalent inhibitors for the SARS-CoV-2 3CL protease, Nat. Commun. 12 (2021) 3623.

[26] J.M. Bradshaw, J.M. McFarland, V.O. Paavilainen, A. Bisconte, D. Tam, V.T. Phan, S. Romanov, D. Finkle, J. Shu, V. Patel, T. Ton, X.Y. Li, D.G. Loughhead, P.A. Nunn, D.E. Karr, M.E. Gerritsen, J.O. Funk, T.D. Owens, E. Verner, K.A. Brameld, R.J. Hill, D.M. Goldstein, J. Taunton, Prolonged and tunable residence time using reversible covalent kinase inhibitors, Nat. Chem. Biol. 11 (2015) 525–531.

[27] A.K. Ghosh, J. Raghavaiah, D. Shahabi, M. Yadav, B.J. Anson, E.K. Lendy, S.I. Hattori, N. Higashi-Kuwata, H. Mitsuya, A.D. Mesecar, Indole chloropyridinyl ester-derived SARS-CoV-2 3CLpro inhibitors: enzyme inhibition, antiviral efficacy, structure-activity relationship, and X-ray structural studies, J. Med. Chem. 64 (2021) 14702–14714.

[28] D. Zaidman, P. Gehrtz, M. Filep, D. Fearon, R. Gabizon, A. Douangamath, J. Prilusky, S. Duberstein, G. Cohen, C.D. Owen, E. Resnick, C. Strain-Damerell, P. Lukacik, C. Covid-Moonshot, H. Barr, M.A. Walsh, F. von Delft, N. London, An automatic pipeline for the design of irreversible derivatives identifies a potent SARS-CoV-2 M^{pro} inhibitor, Cell Chem. Biol. 28 (2021) 1795–1806.

[29] J.K. Stille, J. Tjutrins, G. Wang, F.A. Venegas, C. Hennecker, A.M. Rueda, I. Sharon, N. Blaine, C.E. Miron, S. Pinus, A. Labarre, J. Plescia, M.B. Patrascu, X. Zhang, A.S. Wahba, D. Vlaho, M.J. Huot, T.M. Schmeing, A.K. Mittermaier, N. Moitessier, Design, synthesis and in vitro evaluation of novel SARS-CoV-2 3CLpro covalent inhibitors, Eur. J. Med. Chem. (2021), https://doi.org/10.1016/j.ejmech.2021.114046.

[30] G. Amendola, R. Ettari, S. Previti, C. Di Chio, A. Messere, S. Di Maro, S.J. Hammerschmidt, C. Zimmer, R.A. Zimmermann, T. Schirmeister, M. Zappala, S. Cosconati, Lead discovery of SARS-CoV-2 main protease inhibitors through covalent docking-based virtual screening, J. Chem. Inf. Model. 61 (2021) 2062–2073.

[31] G.M. Sastry, M. Adzhigirey, T. Day, R. Annabhimoju, W. Sherman, Protein and ligand preparation: parameters, protocols, and influence on virtual screening enrichments, J. Comput. Aided Mol. Des. 27 (2013) 221–234.

[32] E. Harder, W. Damm, J. Maple, C. Wu, M. Reboul, J.Y. Xiang, L. Wang, D. Lupyan, M.K. Dahlgren, J.L. Knight, J.W. Kaus, D.S. Cerutti, G. Krilov, W.L. Jorgensen, R. Abel, R.A. Friesner, OPLS3: a force field providing broad coverage of drug-like small molecules and proteins, J. Chem. Theor. Comput. 12 (2016) 281–296.

[33] D. Lagorce, L. Bouslama, J. Becot, M.A. Miteva, B.O. Villoutreix, FAF-Drugs4: free ADME-tox filtering computations for chemical biology and early stages drug discovery, Bioinformatics 33 (2017) 3658–3660.

[34] K. Zhu, K.W. Borrelli, J.R. Greenwood, T. Day, R. Abel, R.S. Farid, E. Harder, Docking covalent inhibitors: a parameter free approach to pose prediction and scoring, J. Chem. Inf. Model. 54 (2014) 1932–1940.

[35] Q.S. Wang, K.H. Zhang, Y. Cui, Z.J. Wang, Q.Y. Pan, K. Liu, B. Sun, H. Zhou, M.J. Li, Q. Xu, C.Y. Xu, F. Yu, J.H. He, Upgrade of macromolecular crystallography beamline BL17U1 at SSRF, Nucl. Sci. Tech. 29 (2018) 1–7.

[36] W. Minor, M. Cymborowski, Z. Otwinowski, M. Chruszcz, HKL-3000: the integration of data reduction and structure solution - from diffraction images to an initial model in minutes, Acta Crystallogr. D Biol. Crystallogr. 62 (2006) 859–866.

[37] A.J. McCoy, R.W. Grosse-Kunstleve, P.D. Adams, M.D. Winn, L.C. Storoni, R.J. Read, Phaser crystallographic software, J. Appl. Crystallogr. 40 (2007) 658–674.

[38] P. Emsley, K. Cowtan, Coot: model-building tools for molecular graphics, Acta Crystallogr. D Biol. Crystallogr. 60 (2004) 2126–2132.

[39] P.D. Adams, R.W. Grosse-Kunstleve, L.W. Hung, T.R. Ioerger, A.J. McCoy, N.W. Moriarty, R.J. Read, J.C. Sacchettini, N.K. Sauter, T.C. Terwilliger, PHENIX: building new software for automated crystallographic structure determination, Acta Crystallogr. D Biol. Crystallogr. 58 (2002) 1948–1954.

[40] Gregory B. Craven, Dominic P. Affron, Charlotte E. Allen, Stefan Matthies, Joe G. Greener, Rhodri M.L. Morgan, Edward W. Tate, Alan Armstrong, David J. Mann, High-throughput kinetic analysis for target-directed covalent ligand discovery, Angew. Chem. Int. Ed. 57 (2018) 5257–5261.

[41] L. Zhang, D. Lin, Y. Kusov, Y. Nian, Q. Ma, J. Wang, A. von Brunn, P. Leyssen, K. Lanko, J. Neyts, A. de Wilde, E.J. Snijder, H. Liu, R. Hilgenfeld, Alpha-Ketoamides as broad-spectrum inhibitors of coronavirus and enterovirus replication: structure-based design, synthesis, and activity assessment, J. Med. Chem. 63 (2020) 4562–4578.

[42] K. Akaji, H. Konno, H. Mitsui, K. Teruya, Y. Shimamoto, Y. Hattori, T. Ozaki, M. Kusunoki, A. Sanjoh, Structure-based design, synthesis, and evaluation of peptide-mimetic SARS 3CL protease inhibitors, J. Med. Chem. 54 (2011) 7962–7973.

[43] H. Wang, S. He, W.L. Deng, Y. Zhang, G.B. Li, J.X. Sun, W. Zhao, Y. Guo, Z. Yin, D.M. Li, L.Q. Shang, Comprehensive insights into the catalytic mechanism of Middle East respiratory syndrome 3C-like protease and severe acute respiratory syndrome 3C-like potease, ACS Catal. 10 (2020) 5871–5890.

[44] P. Abranyi-Balogh, L. Petri, T. Imre, P. Szijj, A. Scarpino, M. Hrast, A. Mitrovic, U.P. Fonovic, K. Nemeth, H. Barreteau, D.I. Roper, K. Horvati, G.G. Ferenczy, J. Kos, J. Ilas, S. Gobec, G.M. Keseru, A road map for prioritizing warheads for cysteine targeting covalent inhibitors, Eur. J. Med. Chem. 160 (2018) 94–107.

[45] R.A. Bauer, Covalent inhibitors in drug discovery: from accidental discoveries to avoided liabilities and designed therapies, Drug Discov. Today 20 (2015) 1061–1073.

[46] L. Petri, P. Abranyi-Balogh, P.R. Varga, T. Imre, G.M. Keseru, Comparative reactivity analysis of small-molecule thiol surrogates, Bioorg. Med. Chem. 28 (2020) 115357.

[47] Y. Shin, J.W. Jeong, R.P. Wurz, P. Achanta, T. Arvedson, M.D. Bartberger, I.D.G. Campuzano, R. Fucini, S.K. Hansen, J. Ingersoll, J.S. Iwig, J.R. Lipford, V. Ma, D.J. Kopecky, J. McCarter, T. San Miguel, C. Mohr, S. Sabet, A.Y. Saiki, A. Sawayama, S. Sethofer, C.M. Tegley, L.P. Volak, K. Yang, B.A. Lanman, D.A. Erlanson, V.J. Cee, Discovery of N-(1-Acryloylazetidin-3-yl)-2-(1H-indol-1-yl)acetamides as covalent inhibitors of KRAS(G12C), ACS Med. Chem. Lett. 10 (2019) 1302–1308.